

Ultra-compact, flat-top demultiplexer using anti-reflection contra-directional couplers for CWDM networks on silicon

Wei Shi,* Han Yun, Charlie Lin, Mark Greenberg, Xu Wang,
Yun Wang, Sahba Talebi Fard, Jonas Flueckiger, Nicolas A. F. Jaeger,
and Lukas Chrostowski

*Department of Electrical and Computer Engineering, University of British Columbia,
Vancouver, BC, Canada*

*weis@ece.ubc.ca

Abstract: Wavelength-division-multiplexing (WDM) networks with wide channel grids and bandwidths are promising for low-cost, low-power optical interconnects. Wide-bandwidth, single-band (i.e., no free-spectral range) add-drop filters have been developed on silicon using anti-reflection contra-directional couplers with out-of-phase Bragg gratings. Using such filter components, we demonstrate a 4-channel, coarse-WDM demultiplexer with flat passbands of up to 13 nm and an ultra-compact size of $1.2 \times 10^{-3} \text{ mm}^2$.

© 2013 Optical Society of America

OCIS codes: (050.2770) Gratings; (130.3120) Integrated optics devices; (230.7370) Waveguides; (130.7408) Wavelength filtering devices.

References and links

1. Y. Vlasov, "Silicon CMOS-integrated nano-photonics for computer and data communications beyond 100G," *IEEE Communications Magazine* **50**, s67–s72 (2012).
2. M. Hochberg and T. Baehr-Jones, "Towards fabless silicon photonics," *Nature Photonics* **4**, 492–494 (2010).
3. W. Shi, R. Vafaei, M. Á. G. Torres, N. A. F. Jaeger, and L. Chrostowski, "Design and characterization of microring reflectors with a waveguide crossing," *Optics Letters* **35**, 2901–2903 (2010).
4. W. A. Zortman, D. C. Trotter, and M. R. Watts, "Silicon photonics manufacturing," *Opt. Express* **18**, 23598–23607 (2010).
5. D. Feng, W. Qian, H. Liang, C.-C. Kung, J. Fong, B. J. Luff, and M. Asghari, "Fabrication insensitive echelle grating in silicon-on-insulator platform," *IEEE Photon. Technol. Lett.* **23**, 284–286 (2011).
6. L. Chen, L. Buhl, and Y. Chen, "Eight-channel $\text{SiO}_2/\text{Si}_3\text{N}_4/\text{Si}/\text{Ge}$ CWDM receiver," *IEEE Photon. Technol. Lett.* **23**, 1201–1203 (2011).
7. J. Brouckaert, G. Roelkens, S. K. Selvaraja, W. Bogaerts, P. Dumon, S. Verstyuyt, D. V. Thourhout, and R. Baets, "Silicon-on-insulator CWDM power monitor/receiver with integrated thin-film InGaAs photodetectors," *IEEE Photon. Technol. Lett.* **21**, 1423–1425 (2009).
8. P. J. Bock, P. Cheben, J. H. Schmid, A. V. Velasco, A. Delâge, S. Janz, D.-X. Xu, J. Lapointe, T. J. Hall, and M. L. Calvo, "Demonstration of a curved sidewall grating demultiplexer on silicon," *Optics Express* **20**, 19882–19892 (2012).
9. P. Yeh and H. F. Taylor, "Contradirectional frequency-selective couplers for guided-wave optics," *Appl. Opt.* **19**, 2848–2855 (1980).
10. W. Shi, X. Wang, C. Lin, H. Yun, Y. Liu, T. Baehr-Jones, M. Hochberg, N. A. F. Jaeger, and L. Chrostowski, "Silicon photonic grating-assisted, contra-directional couplers," *Optics Express* **21**, 3633–3650 (2012).
11. W. Shi, X. Wang, W. Zhang, H. Yun, C. Lin, L. Chrostowski, and N. A. F. Jaeger, "Grating-coupled silicon microring resonators," *Appl. Phys. Lett.* **100**, 121118 (2012).
12. D. T. H. Tan, K. Ikeda, S. Zamek, A. Mizrahi, M. P. Nezhad, A. V. Krishnamoorthy, J. E. C. K. Raj, X. Zheng, I. Shubin, Y. Luo, and Y. Fainman, "Wide bandwidth, low loss 1 by 4 wavelength division multiplexer on silicon for optical interconnects," *Optics Express* **19**, 2401–2409 (2011).

13. W. Shi, M. Greenberg, X. Wang, C. Lin, N. A. F. Jaeger, and L. Chrostowski, "Single-band add-drop filters using anti-reflection, contradirectional couplers," IEEE Group IV Photonics Conference (San Diego, CA, USA 2012), paper WA7.
 14. H. Qiu, G. Jiang, T. Hu, H. Shao, P. Yu, J. Yang, and X. Jiang, "FSR-free add-drop filter based on silicon grating-assisted contradirectional couplers," Optics Letters **38**, 1–3 (2013).
 15. W. Shi, X. Wang, W. Zhang, L. Chrostowski, and N. A. F. Jaeger, "Contradirectional couplers in silicon-on-insulator rib waveguides," Optics Letters **36**, 3999–4001 (2011).
-

1. Introduction

Broadband optical communications for Internet data centres and high-performance communications have been a significant driving force for silicon photonics [1], which is promising for large-scale electronic-photonics integration [2]. For these applications, wavelength-division multiplexing (WDM) networks are promising, if not necessary, to satisfy ever increasing demands for bandwidth [1]. One of the main challenges facing WDM systems on silicon lies in the wavelength drift due to the high thermal sensitivity of the effective indices [3] and the fabrication-induced non-uniformity [4] of silicon optical waveguides. It is anticipated that frequency trimming/tuning will take a significant portion of the overall power budget of a silicon photonic chip [4]. This has been a big issue, since power efficiency (J/bit) is one of the most important criteria for short-reach communications. WDM technologies with wide channel grids within a broad band, e.g., coarse WDM (CWDM), can tolerate higher temperature fluctuations and fabrication errors and, therefore, may be more promising as compared to finer-grid technologies, e.g., dense WDM (DWDM), for above mentioned applications in the near future. High-performance CWDM demultiplexers have been demonstrated on silicon using echelle and arrayed waveguide gratings [5, 6], nevertheless, these devices are relatively bulky (on a scale of 10 mm²). Compact demultiplexers, smaller than 0.1 mm², were recently demonstrated for CWDM networks on the sub-micron silicon platform, e.g., using planar concave gratings [7] or curved sidewall gratings [8]. However, these devices do not have flat-top responses and, therefore, still have challenges to achieve reliable operation without thermal control.

Here, we demonstrate a CWDM demultiplexer using anti-reflection (AR) contra-directional couplers (contra-DCs). Contra-DCs are add-drop filters with Bragg-grating defined wavelength-selective functions [9, 10]. Compared to add-drop filters using microring resonators, contra-DCs do not have the issue of multiple longitudinal modes [11] and can provide wider channel bandwidths [10]. For example, a 4-channel demultiplexer using cascaded contra-DCs was recently demonstrated with a 3-nm channel bandwidth and a 6-nm channel spacing [12]. However, these contra-DCs suffer from back reflections which limit their usable spectral ranges (20 ~ 40 nm) and make them unsuitable for CWDM networks which require a broad spectrum of > 100 nm and a wide channel spacing of 20 nm. To overcome this issue, we proposed and demonstrated an anti-reflection (AR) design using out-of-phase gratings, which enabled a single-band (no FSR), wide-bandwidth add-drop filter [13]. In this paper, we firstly describe the principle of AR contra-DCs in comparison with a conventional contra-DC. Then, we extend the concept to a dual-coupler structure and demonstrate an ultra-compact, 4-channel demultiplexer with wide passbands (> 10 nm) and flat-top responses for CWDM networks.

As shown in Fig. 1(a), a conventional contra-DC consists of two optical waveguides with dielectric perturbations, i.e., Bragg gratings, formed in the coupling region. The two waveguides have different widths and, thus, different propagation constants. This asymmetric coupler design results in very weak co-directional coupling due to the phase mismatch. The grating pitch, Λ , is chosen so that efficient contra-directional coupling occurs between the first two transverse modes (supermodes), \mathbf{E}_1 and \mathbf{E}_2 , of the coupler at the drop-port central wavelength, λ_D , which satisfies the phase-match condition [9], i.e., $\lambda_D = 2n_{av}\Lambda$, where $n_{av} = (n_1 + n_2)/2$ and n_1 and n_2 are the effective indices of the two modes. Coupling between the forward and backward

propagating waves of each mode (i.e., back reflection) also exists centred at the Bragg wavelength, i.e., $\lambda_{r1,2} = 2n_{1,2}\Lambda$. The spacing between λ_D and λ_{r2} (or λ_{r1}) limits the usable spectral range and may distort the filter response [10]. Figure 1(b) shows the mode distributions and effective indices of a contra-DC simulated using a mode solver with the designed parameters given below in next section. Each supermode has its energy localized to one waveguide due to the high coupler asymmetry [10], as opposed to a symmetric directional coupler where the energy is present in both waveguides. Using the phase-match conditions, we can find the central wavelengths, as labeled in Fig. 1(b). The back reflection can be reduced by putting the dielectric perturbation away from the input waveguide (e.g., by forming the grating only on the drop waveguide and using a large coupler gap [14]). However, this is unsuitable for wide-bandwidth filters (that require large perturbations and narrow coupler gaps for strong coupling) and would still have strong reflection for “add” or multiplexing operation (i.e., combining optical signals through the add port).

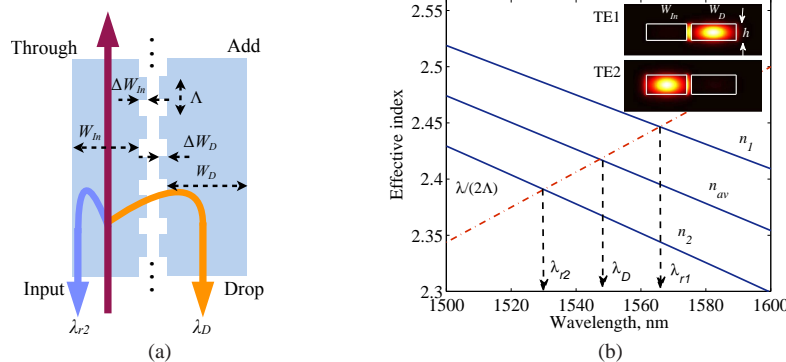


Fig. 1. (a) Schematic of a conventional contra-DC; (b) Calculated effective indices of the first two TE-like modes in the device illustrated in (a). The insets are the calculated intensity distributions of the electric fields for the two modes.

2. Anti-reflection, contra-directional couplers

In order to extend the usable spectral range for CWDM networks, we proposed using out-of-phase gratings to suppress the back reflections [13]. Using sidewall gratings as an example, the schematic of an AR contra-DC is shown in Fig. 2(a). Compared to the structure shown in Fig. 1(a), the AR contra-DC has extra gratings (AR gratings) formed on the external sides of the waveguides. The AR gratings are designed to have a $\Lambda/2$ mismatch with respect to the gratings in the coupler region. As a result of destructive interference, the back reflections of each mode can be significantly suppressed. Since inter-waveguide coupling relies on the perturbations between the waveguides, efficient contra-directional coupling can be maintained even in the presence of AR gratings. In contrast to AR coatings where $1/4$ -lambda-thick materials are used for destructive interference, here, the AR effect is implemented by creating a grating structure such that its effective index is constant in the propagation direction. From the perspective of coupled-mode theory, the coupling efficiency depends on the overlap of \mathbf{E}_1 and \mathbf{E}_2 with the dielectric perturbation [9, 10]. Therefore, to achieve complete destructive interference, each mode should see the same magnitudes of the perturbations due to the AR gratings and coupler gratings. Because each mode is not symmetric with respect to the centre of each waveguide, the grating widths and coupler gaps should be carefully designed to balance the magnitudes of the perturbations. Also, it is worth pointing out that this concept of AR gratings can be easily transferred into contra-DCs based on cladding- or slab-modulated rib waveguide structures [15].

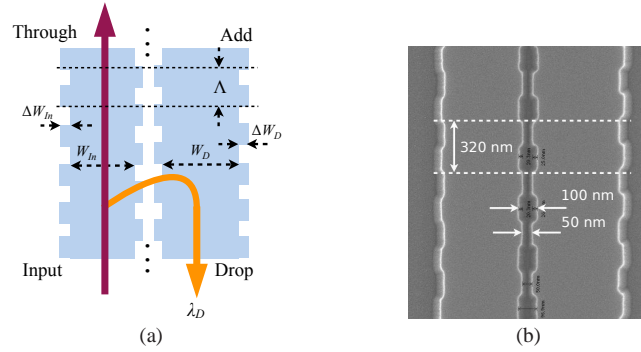


Fig. 2. (a) Schematic of an AR contra-DC; (b) SEM image of a fabricated AR contra-DC.

The designed contra-DCs were fabricated using e-beam lithography and plasma etch to verify the concept of AR gratings, as previously reported in [13]. The devices are in 220-nm-high silicon-on-insulator waveguides without top cladding. The widths of the input and drop waveguides, W_{In} and W_D , are 450 and 500 nm, respectively. The gratings are formed by corrugating the side-walls of strip waveguides, with a 320-nm pitch, a 50% duty cycle, and 800 periods. The corrugation widths on W_{In} and W_D are 20 and 30 nm, respectively. The average gap between the waveguides is 75 nm. An SEM image of a fabricated AR contra-DC is shown in Fig. 2(b).

We measured the through-port spectra of the contra-DCs. As seen in Fig. 3(a), there are two notches (stop bands) in the spectrum of the device without the AR gratings. The first notch at 1528 nm (λ_{r2}) is due to the back reflections of \mathbf{E}_2 . The second notch at 1550 nm (λ_D) corresponds to the contra-directional coupling between \mathbf{E}_1 and \mathbf{E}_2 . Thus, the spectral range between λ_D and λ_{r2} in this case is about 20-nm wide, in good agreement with the calculation shown in Fig. 1(b). In contrast, in the spectrum of the AR contra-DC shown in Fig. 3(b), only one stop band at λ_D can be identified within a broad spectrum across 180 nm, i.e., the entire span of the tunable laser used for the measurement. This single stop band shows a wide bandwidth of 6.5 nm and a high extinction ratio of 20 dB, indicating that the back reflections have been significantly suppressed, while a strong contra-directional coupling remains.

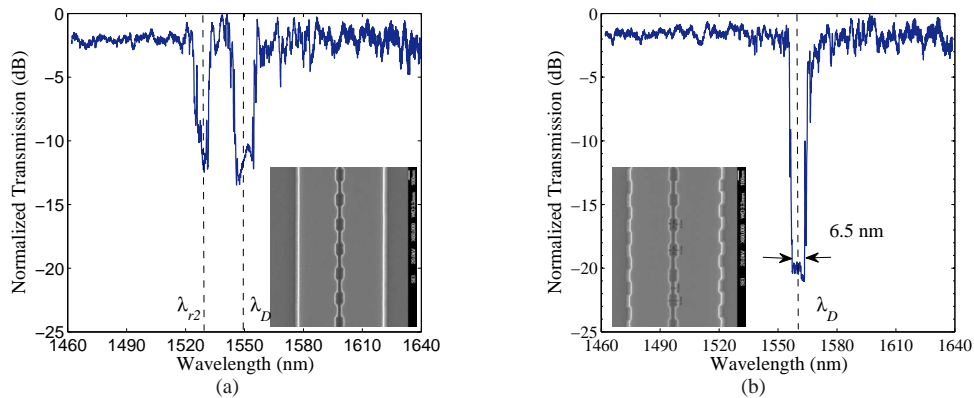


Fig. 3. Measured through-port optical spectra: (a) conventional contra-DC without the AR gratings; (b) AR contra-DC. The insets are the SEM images of the devices.

3. CWDM demultiplexer

Using the AR contra-DCs, we developed a 4-channel CWDM demultiplexer, for which a schematic is shown in Fig. 4. In order to obtain a more compact device, the contra-DCs are designed in pairs using a dual-coupler structure (i.e., a three-waveguide structure [9, 12]). Each coupler pair has two drop waveguides with different waveguide widths ($W_1 = 470$ nm and $W_2 = 560$ nm), but, the same grating pitch. The input waveguide has a width, W_{in} , of 420 nm. It is important to note that the gratings on opposite sides of each waveguide are out of phase to suppress the back reflections. The amplitudes of the side-wall corrugations on W_{in} , W_1 , and W_2 are designed to be 30, 40, and 50 nm, respectively. The average coupler gaps between W_1 and W_{in} and between W_2 and W_{in} are 115 and 120 nm, respectively.

The demultiplexing function is related to the first three TE-like modes (supermodes) of the dual-coupler structure, i.e., \mathbf{E}_1 , \mathbf{E}_2 , and \mathbf{E}_3 , which are mainly confined within W_2 , W_1 , and W_{in} , respectively. The calculated electric-field intensity distributions are shown in Fig. 5(a). Each coupler pair drops two wavelengths; one corresponds to the coupling between \mathbf{E}_3 and \mathbf{E}_2 and the other corresponds to the coupling between \mathbf{E}_3 and \mathbf{E}_1 . The parameters mentioned above ensure that the magnitudes of the perturbations, due to the gratings on both sides of the input waveguides, seen by the input mode (\mathbf{E}_3) would be the same.

The 4-channel demultiplexer was implemented by cascading two pairs of such dual-coupler filters. The grating pitches of the first pair (Drop 1 and 2) and second pair (Drop 3 and 4) are designed to be Λ_1 (325 nm) and Λ_2 (340 nm), respectively. The dropped wavelengths predicted using the phase-match conditions, as shown in Fig. 5(b) (where $n_{av1} = (n_3 + n_2)/2$ and $n_{av2} = (n_3 + n_1)/2$ have been used), range from 1530 nm to 1590 nm with spacings of 20 nm between adjacent channels. One thousand grating periods have been used for each of the contra-DCs. The total length of the coupling regions, including both the coupler pairs, is 665 μm . The total area of the four contra-DCs, not including the routing waveguides, is less than 1.2×10^{-3} mm^2 .

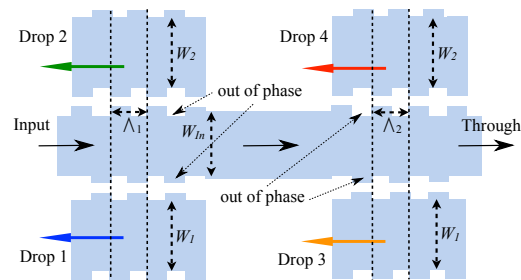


Fig. 4. Schematic of a demultiplexer using AR contra-DCs.

The designed demultiplexer was fabricated using the same e-beam lithography and plasma etch process. An SEM image of the device is shown in Fig. 6(a). The measured spectra of the demultiplexer are plotted in Fig. 6(b). The channel bandwidths are in a range of 11 to 13 nm. Taking the typical wavelength dependence of 0.09 nm/K on temperature [3], we expect that these wide passbands will allow a temperature swing of ± 60 K. Insertion loss is less than 1 dB for each channel. Channel crosstalk is better than -12 dB and is limited by the strong sidelobes and the residual co-directional couplings, which can be improved upon by using apodization techniques and adiabatic tapers between the individual waveguides and the coupler regions [10]. The zoomed spectrum of the second channel is shown in Fig. 6(c), in comparison with simulation using the coupled-mode analysis [10], indicating a flat-top response. The ripples within the passband are likely due to the relatively large shot-pitch grid (6 nm) used in the e-beam lithography and can be suppressed by using a finer grid (e.g., 2 nm) and apodization.

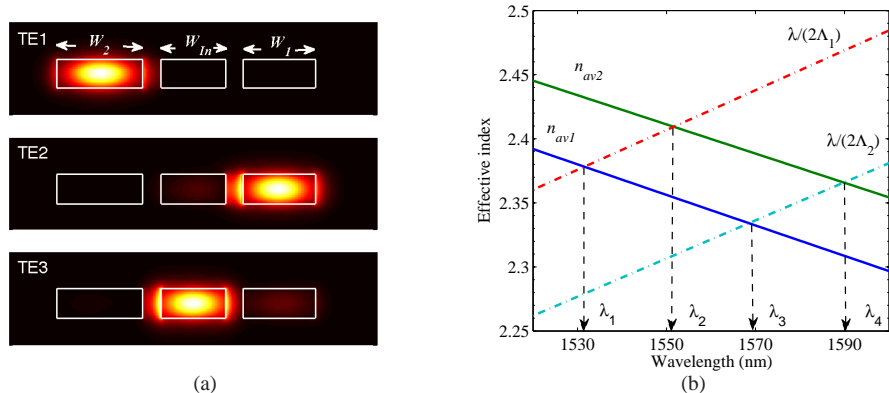


Fig. 5. Calculated electric-fields of the first three TE-like modes of an AR contra-DC with a dual-coupler structure: (a) intensity distributions at 1560 nm; (b) average effective indices and predicted central wavelengths of the demultiplexer.

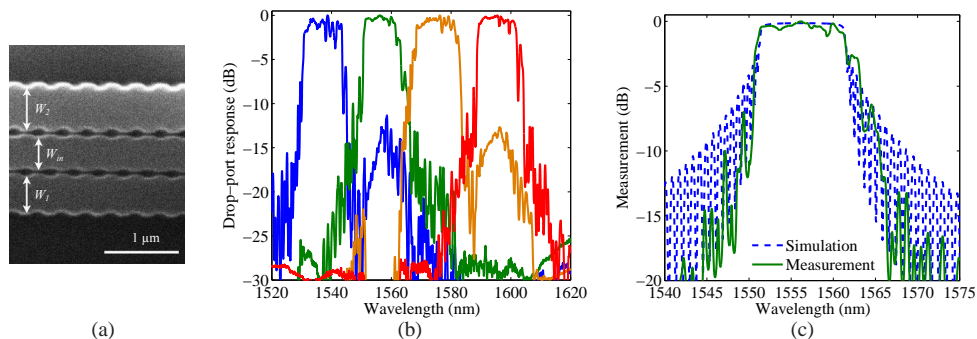


Fig. 6. (a) SEM image of a pair of AR contra-DCs; (b) drop-port responses of a 4-channel CWDM demultiplexer; (c) measured and curve-fit spectra of the second channel.

4. Conclusion

We have demonstrated silicon AR contra-DCs using out-of-phase gratings to significantly extend their usable spectral ranges. A wide-bandwidth add-drop filter, with single-band operation (i.e., without an FSR) has been obtained in a wide spectral span of 180 nm. Using such AR contra-DCs, we have achieved a 4-channel CWDM demultiplexer with flat-top passbands, channel bandwidths of up to 13 nm, and an effective area as small as $1.2 \times 10^{-3} \text{ mm}^2$. We expect that it can also perform as a multiplexer by using the add ports as inputs. These wide-bandwidth WDM filters are highly tolerant to temperature fluctuations and have great potential for low-cost, power-efficient WDM networks using CMOS-compatible photonic technology.

Acknowledgement

We acknowledge Lumerical Solutions, Inc. for the design software (MODE Solutions) and the Natural Sciences and Engineering Research Council of Canada for their financial support. Fabrication was conducted at the University of Washington Microfabrication/Nanotechnology User Facility, a member of the NSF National Nanotechnology Infrastructure Network.